Progress on development of an airborne two-micron IPDA lidar for water vapor and carbon dioxide column measurements

Upendra N. Singh*[a], Mulugeta Petros[a], Tamer F. Refaat[a], Jirong Yu[a], Charles W. Antill[a], Bryant D. Taylor[b], Stephen C. Bowen[a], Angela M. Welters[a], Ruben G. Remus[a], Teh-Hwa Wong[b], Karl Reithmaier[b], Jane Lee[b] and Syed Ismail[c]
[a]NASA Langley Research Center, Hampton, VA, USA 23681; [b]Science Systems and Applications, Inc., Hampton, VA, 23666; [c]Analytical Services and Materials, Inc., Hampton, VA, 23666.

ABSTRACT

An airborne 2-μm triple-pulse integrated path differential absorption (IPDA) lidar is currently under development at NASA Langley Research Center (LaRC). This lidar targets both atmospheric carbon dioxide (CO_2) and water vapor (H_2O) column measurements, simultaneously. Advancements in the development of this IPDA lidar are presented in this paper. Updates on advanced two-micron triple-pulse high-energy laser transmitter will be given including packaging and lidar integration status. In addition, receiver development updates will also be presented. This includes a state-of-the-art detection system integrated at NASA Goddard Space Flight Center. This detection system is based on a newly developed HgCdTe (MCT) electron-initiated avalanche photodiode (e-APD) array. Future plan for IPDA lidar system for ground integration, testing and flight validation will be discussed.

Keywords: Active remote sensing, carbon dioxide, water vapor, integrated path differential absorption lidar

1. INTRODUCTION

Understanding the carbon dioxide (CO_2) exchange processes, in the context of global climate change, has become an important topic to the scientific community. Knowledge of the spatial and temporal distribution of CO_2 sources and sinks, and transport on global scales, are critical to predict, and possibly manage, the carbon cycle and radiation budget processes. In response to these challenges, laser-based active optical remote sensing is considered for mapping atmospheric CO_2 using airborne and space-based platforms [1]. Active remote sensors have a number of advantages including night, seasonal, high latitude, and tropical ecosystems measurements. Several differential absorption lidar (DIAL) based CO_2 active remote sensing instruments have been developed at NASA Langley Research Center (LaRC) [2-6]. These instruments focus on pulsed 2-μm transmitters, which provide direct range measurement including absorption column length. The 2-μm region offers attractive spectroscopic features that include strong CO_2 absorption, low temperature dependence and minor interference from other atmospheric gases. In addition, for Integrated Path Differential Absorption (IPDA) lidar application, the 2-μm favors low tropospheric weighting functions that focus on CO_2 near-surface dynamics.

Recently, an airborne 2-μm high-energy, double-pulse, direct detection IPDA lidar have been integrated and validated at LaRC for CO_2 measurements [5-9]. This double-pulse IPDA was tuned around the CO_2 R30 strong absorption line at 2050.9670 nm. Airborne field experiments were conducted to quantify and characterize instrument capabilities, sensitivity and bias errors by comparison to performance models. Double-pulse IPDA range measurements from ground indicated a 0.93 m uncertainty, which is limited by the 200 ns transmitted laser pulse and detection system bandwidth. This uncertainty increased to 2.80 and 7.40 m over ocean and land, due to fluctuations in ocean surface and ground elevations, respectively [5, 8-9]. CO_2 differential optical depth measurements by the IPDA agree with models. For example, CO_2 differential optical depth measurements over ocean from 3.1 and 6.1 km altitudes indicated 0.95% and 0.83% uncertainty, respectively, using 10 second (100 shots) averaging. Using the same averaging 0.40% uncertainty was observed over land, from 3.4 km altitude, due to higher surface reflectivity, which increases the return signal power and enhances the signal-to-noise ratio. However, less uncertainty is observed at higher altitudes due to reduced signal shot noise, indicating that detection system noise-equivalent-power dominates the error. These results show that the IPDA technique is well suited for high altitude operation such as space-based platforms. High altitude operation includes integration of larger column content that enhances measurement sensitivity.

Currently, through continual support from the NASA Earth Science Technology Office (ESTO), a 2-μm triple-pulse IPDA is under development at LaRC [10-12]. This triple-pulse IPDA will allow simultaneous and independent measurement of water vapor (H_2O) and CO_2 differential optical depths from an airborne platform. This system is a technological upgrade to the knowledge gathered through the 2-μm CO_2 double-pulse IPDA lidar system. This triple-pulse IPDA lidar is a direct detection system based on a state-of-the-art high repetition rate (50 Hz), high-energy (80 mJ), triple-pulse, 2-μm laser transmitter. The updated status of the triple-pulse IPDA development is presented in this paper. This includes updates on the state-of-the-art triple-pulse laser transmitter, seed laser locking, wavelength control, receiver telescope, detection system and data acquisition. This novel instrument allows measurement of the two most dominant greenhouse gases, simultaneously and independently, using a single instrument. Therefore, the design of this airborne triple-pulse IPDA lidar instrument enables technology development for future space-based system for global CO_2 measurement, while reducing risk, cost, size, volume, mass and development time of required sensor [13].

2. IPDA LIDAR TRANSMITTER

In this triple-pulse IPDA lidar, the 2-μm laser transmitter emits three successive pulses separated by 200 μs at 50 Hz repetition rate. Short time separation between the IPDA transmitted pulses maximizes the measured column volume-overlap and surface footprint. These pulses are seeded at selected wavelengths that are generated by a frequency offset with respect to the CO_2 R30 line center. The transmitter is co-axially aligned to the receiver telescope through bore-sighting. The IPDA receiver system is similar to the successfully demonstrated 2-μm CO_2 double-pulse IPDA [5-6].

2.1 Triple-Pulse Laser

The IPDA 2-μm laser transmitter is based on Ho:Tm:YLF crystal with an emitted radiation wavelengths that cover strong CO_2 absorption features. The long upper laser level lifetime of Tm and Ho provides the capability of generating three Q-switched pulses using a single pump pulse. The crystal is end pumped using 792 nm to excite the Tm. The excited Tm pumps the Ho, which generates the 2-μm emission. The co-doped approach has the advantage of providing close to twice the quantum efficiency in the Tm, and overall system simplicity [14]. Table 1 lists the IPDA lidar transmitter development progress efforts by observing the enhancement of the generated pulse energies as compared to the initial goals. Several tradeoffs between different laser performance parameters and design configuration were considered. This includes pumping configuration, oscillator type, doping concentrations, crystal dimensions, diffusion bonding and thermal loading, in addition to procurement challenges, integration and testing. The laser operation is digitally controlled through a computer using the laser timing control (LTC) unit interface, shown in figure 1. All required electronics for laser operation and control were integrated in the LTC unit. These include pulse timing electronics, Q-switch deriver and synchronization signals. A Graphical User Interface (GUI) controls the laser operation through selecting and controlling different aspects of the laser operation, such as the number of produced pulses, timing between pulses, wavelength selection for each pulse and pulse rate.

The operation and control of this unit was tested successfully using the double-pulse IPDA (i.e., triple-pulse operation of the double pulse IPDA) in the mobile lidar laboratory. This unit is three times lighter and more compact than what was developed in double-pulse IPDA. The triple-pulse laser oscillator was integrated and final thermal analysis and alignment optimization is currently on going to enhance the performance. The LTC unit was also tested successfully with the new triple-pulse laser oscillator. Figure 2 shows the temporal variation of the triple-pulse generation event. Stable pulse energy output is observed as shown in figure 3. Heat accumulation is a major challenge limiting the 2-μm output energy and stability and can result in crystal damage. Thus, heat dissipation is essential for high intensity pump where high repetition rate operation is required. This required additional mitigation strategies for the laser head design.

Table 1. Progress of the IPDA lidar transmitter pulse energy distribution through current developments as compared to the initial goals.

	February, 2016	April, 2016	November, 2016	Goal
First Pulse	20 mJ	20 mJ	40 mJ	50 mJ
Second Pulse	7 mJ	12 mJ	26 mJ	15 mJ
Third Pulse	7 mJ	11 mJ	14 mJ	5 mJ
Total	34 mJ	42 mJ	80 mJ	70 mJ

The laser head is designed to conductively cool the laser crystal. The laser crystal is wrapped with thin indium film and mounted in a liquid cooled copper heat sink set to 284K. Thermal analysis was conducted to investigate the proper heat dissipation rate out of the laser crystal. Table 2 lists the main parameters of the IPDA laser transmitter [15].

Figure 1. Frontal picture of the triple-pulse IPDA Laser Timing Control (LTC) unit (bottom) and Wavelength Control Unit (WCU) (top) packaged end-products. Both units are rack mountable, flight hardened, and were tested successfully.

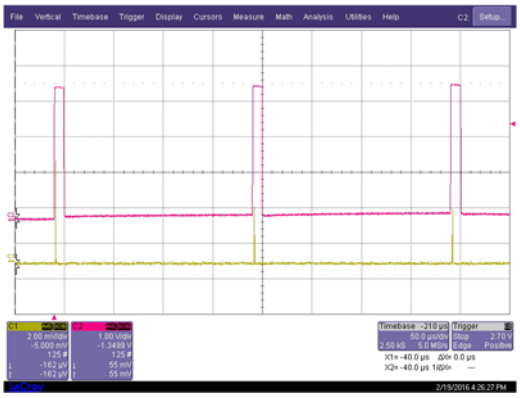

Figure 2. An oscilloscope record of the temporal profile of the triple-pulse generation (yellow) as compared to the Q-switch timing signal (red).

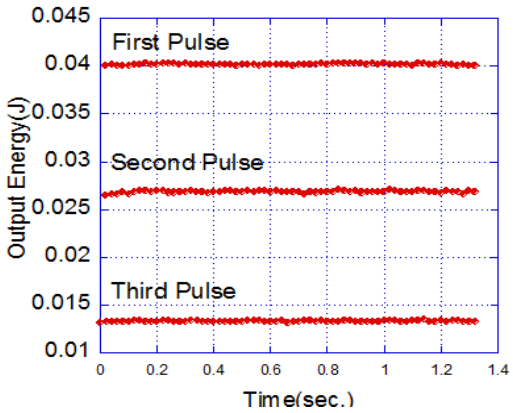

Figure 3. Time record for the shot-by-shot variation of the energy of the individual pulse energies. This energy monitoring capability will be calibrated and integrated within the transmitter enclosure.

Table 2. Parameters of the triple-pulse IPDA lidar transmitter.

	Pulse 1	Pulse 2	Pulse 3
Operating Wavelength (nm)	2050.5094	2051.0590	2051.1915
Frequency Shift (GHz)	+32.6129	-6.5568	-15.999989
Output Energy (mJ)	40	26	14
Pulse width (ns)	22	32	60
Line Width	Transform Limit		
Beam Quality	< 2		
Frequency Accuracy	< 1 MHz		

2.2 Wavelength Control

A wavelength control unit (WCU), shown in figure 1, provides the seeding wavelengths for the 2-µm triple-pulse laser with a required accuracy less than ±1 MHz [16]. This unique wavelength control uses a single cw seed semiconductor laser at 2-µm. This fiber-coupled seed laser was developed at NASA Jet Propulsion Laboratory (JPL) [17]. The wavelength of this laser is locked with reference to the CO_2 R30 line center using an absorption gas cell. The laser, current driver and temperature control, and locking electronic packages are shown in figure 4a. Duplicate electronics were integrated for two devices. The WCU can provide any frequency setting within 35 GHz from the reference. The WCU CW output can be switched between three different frequencies, offset with respect to the locked center line, to provide the three seeding wavelengths, listed in Table 2. The WCU includes several electronic, optical and electro-optical components. The setup for the CO_2 absorption line center locking is shown in figure 4b.

The seed laser output is split into 10% and 90% beams. The 10% beam is modulated with a 200 MHz electro-optics modulator. Center line locking electronics drives the modulator to generate two wavelengths offsets ±2.78 pm from CO_2 line center. The modulated output is collimated and applied to the CO_2 gas cell. The cell output is detected and fed back to the center line locking electronics to sense the error signal. The center line locking controls the laser diode current driver, through the servo signal, to precisely lock the device output wavelength. Statistical analysis of the locked center line wavelength resulted in ±650.1 kHz jitter, which is better than the projected jitter of ±1 MHz. Once the center line is locked, the 90% beam passes through another unit to produce the required side lines, which are set to the 32, -6 and -16 GHz with reference to the R30 line. Figure 5 shows the side line seeding wavelength generation results, as compared to the CO_2 and H_2O absorption spectra.

The system timing is synchronized by the TLC. Q-switch triple-trigger, relative to the pump pulse, produces three successive 2-µm laser pulses with controlled energies and pulse-widths. The pulsed laser is injection seeded with the three different wavelengths by ramp-and-fire method, as shown in figure 6.

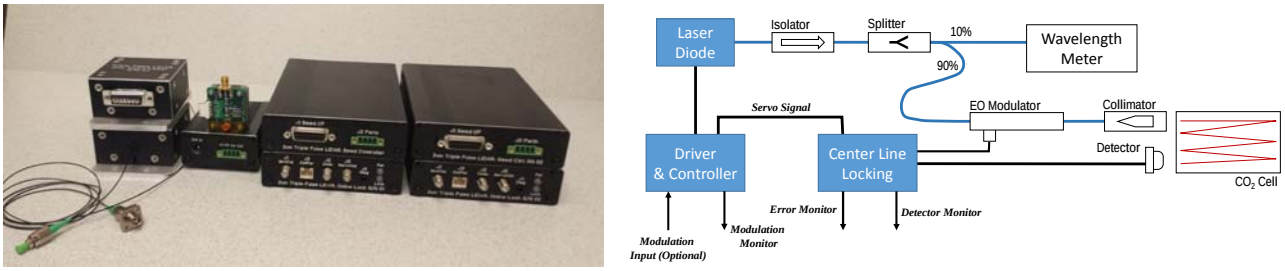

(a) (b)

Figure 4. (a) Packaged laser diode enclosure, laser diode current driver and temperature controller units, and center line locking units. (b) Schematic of the CO_2 absorption line center locking setup. Center line locking electronics drives a 200 MHz EO modulator to generate two wavelengths offsets. Modulated output is collimated and applied to the CO_2 cell, the output of which is detected and feedback to center line locking electronics, which controls the laser diode current through servo enable signal.

The first pulse is tuned to 32 GHz is designed to produce higher energy to accommodate H_2O high absorption loss in online tuning. The second pulse, at -6 GHz, is set to medium lower energy to accommodate CO_2 absorption loss, which is less than H_2O due to lower mixing ratio. In addition, the same pulse acts as the H_2O off-line wavelength. The third pulse, at -16 GHz, with the lowest energy setting serves as the CO_2 off-line. These settings can be altered depending on the required measurement objectives. For example, all pulses could be tuned to the off-line to conduct off-off-line testing [5]. Figure 7 compares the temporal profile of the first pulse output with and without seeding. This indicates the successful operation of the triple-pulse IPDA transmitter.

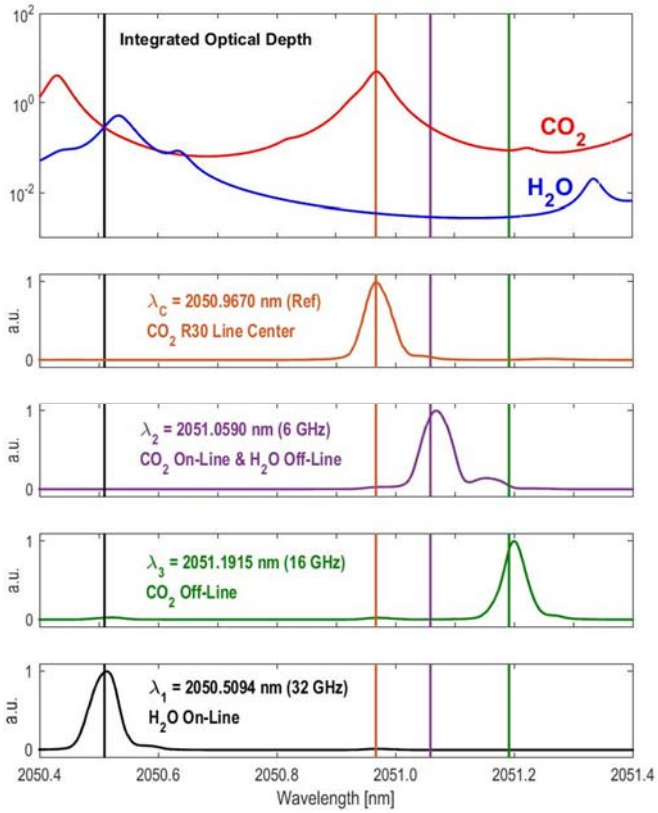

Figure 5. Comparison between the CO_2 and H_2O absorption spectra (Top) and the generated seeding wavelengths for 32, -16 and -6 GHz, as well as the center line locking wavelength (from bottom). Seeding wavelength records were obtained using and Optical Spectrum Analyzer, for verification, with limited resolution of 50 pm that tend to broad the actual spectral line width of the laser.

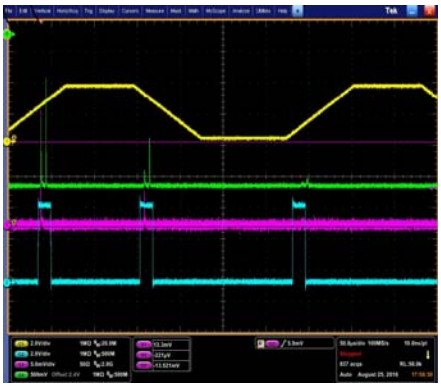

Figure 6. An oscilloscope record for the LTC and WCU synchronization using the Q-switch enable signal (blue). The ramp signal (yellow) is used for injection seeding by the ramp-and-fire method. Energy monitor (red) and target return (green) signals are digitized and recorded using the IPDA data acquisition system.

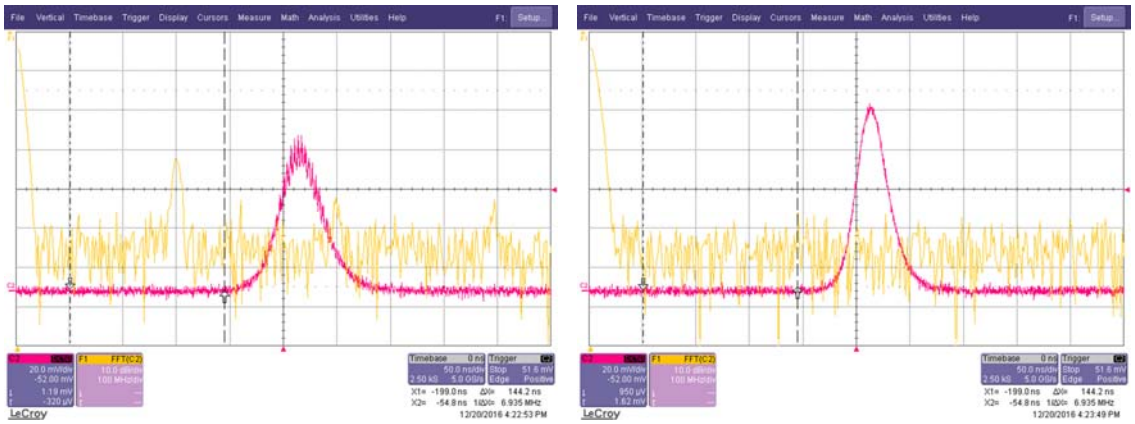

Figure 7. An oscilloscope records comparing the temporal profiles (red) and frequency spectrum (yellow) of the un-seeded (left) and seeded (right) pulsed laser output. These records were obtained for the first pulse.

3. IPDA LIDAR RECEIVER

The 2-μm triple-pulse IPDA lidar receiver, shown schematically in figure 8, consists of a telescope that focuses the return radiation onto aft-optics. The aft-optics collimates and filters the radiation before splitting. The beam splitter generates two optical channels. The first optical channel is a high signal channel with 90% of the radiation applied to a focusing lens on to a 300 μm diameter InGaAs pin detector (Hamamatsu; G5853). The detector output is amplified through a trans-impedance amplifier (TIA). The TIA has the capability to adjust the feedback gain and detection bandwidth. This detection channel is an exact replica to the successful double-pulse IPDA instrument. Since this channel was demonstrated for CO2 measurements, it is included as a reference. The second low signal channel, with 10% radiation, is focused down to an optical fiber that couples the radiation onto a newly-developed detection system by NASA Goddard Space Flight Center (GSFC). This detection system is based on MCT electron-initiated avalanche photodiode (e-APD) detector [18]. The IPDA detected signals are digitized and stored in a state-of-the-art data acquisition unit. The completed triple-pulse IPDA data acquisition software includes data reduction algorithm that is based on sample averaging, which result in virtual sampling rate reduction. Work is currently focused on real time data processing that allows data storage either in raw format, processed format or both.

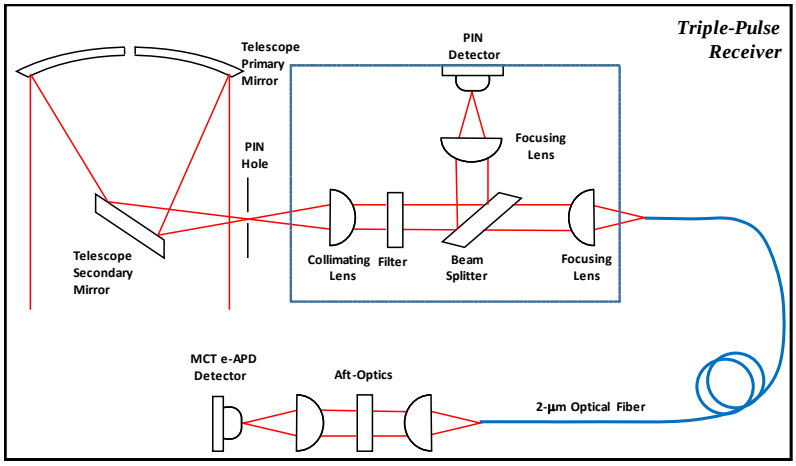

Figure 8. Integrated 2-μm triple-pulse IPDA receiver system based on the previous double-pulse system design. The receiver consists of a telescope, aft optics with high-signal InGaAs channel and low-signal e-APD channel. The e-APD channel is coupled through an optical fiber through additional aft-optics.

3.1 Receiver Optics

The receiver telescope is a Newtonian type with 0.4 m diameter aluminum primary mirror. The shape of the primary mirror is hyperbolic to minimize the aberration and to focus the return signal to less than 300-μm diameter spot size. The telescope is designed to maintain the focus point position in the temperature range between 5 and 35°C. The telescope secondary mirror is a two-surfaces fused silica dichroic flat that turns the return radiation 90° to the side integrated aft-optics from one surface. The opposite surface is used to transmit the expanded laser beam coaxially with the telescope. A single automated mount is used for bore-sight alignment. The primary goal of the telescope integration is to assemble the various parts without any undue stresses. The stress level, mainly due to the primary mirror weight, was measured at a wavelength accuracy and was recorded before and after the assembly. The focal point of the telescope was measured and the position was identified using a 300-μm diameter pinhole that was placed at the focal point. A simple geometric alignment procedure was established to verify consistent telescope alignment after shipping to LaRC from the manufacturer. That included an integrated vibration monitor that was attached to the structure.

3.2 Detection Systems and Data Acquisition

Recent development of advanced single-charge-carrier, HgCdTe e-APD indicated a breakthrough in low-noise lidar detection technology [19]. These devices are space-qualifiable and were validated for airborne lidar operation at 1.6-μm at GSFC. MCT e-APD are sensitive to IR radiation up to 4-μm. Therefore, a cold narrow band-pass filter is desired to limit the device background. In co-ordination with ESTO, LaRC collaborated with GSFC to integrate the detector into the triple-pulse 2-μm IPDA lidar low signal channel. This e-APD comes with 4×4 pixel format (80×80 μm^2 per pixel area) with read-out electronics that enable access to each pixel through individual TIA elements. An output summing amplifier produces the sum of specific number of pixels as selected by the operator. The detector is integrated inside a vacuum chamber, shown in figure 9, which allows cooling the device using a cryo-cooler down to about 77 K to reduce dark current and noise. The e-APD and readout electronics are integrated inside a rack mountable box, shown in figure 9, which includes vacuum setup for thermal isolation. Additional custom designed aft-optics allow focusing the radiation onto 2×2 pixels. The e-APD custom aft-optics is coupled to the IPDA aft-optics through a 2-μm optical fiber, as shown in figure 8. Work efforts at GSFC included 2-μm cold filter integration to the detector chamber, detector assembly testing, and additional aft-optics design with optical fiber coupling. Combining the 2-μm triple-pulse transmitter with this new detection system in a single instrument will result in a new enabling IPDA lidar technology for space based CO_2 measurements [13].

The data acquisition unit is based on two similar high-performance 12-bits digitizers (Agilent; U5303A). These two-channel digitizers operate at a fixed sampling rate of 1 GS/s and they are triggered from the laser Q-switch. One digitizer is dedicated to the IPDA target return signals, with a variable record length of about 70k samples. The other digitizer is dedicated to the laser energy monitors, with a fixed record length of 10k. Using these digitizers is another major enhancement of the triple-pulse IPDA over the double-pulse. Although, digitized data have 12-bit resolution, data storage is achieved in byte increments, leading to 16-bit data records. This indicates that 25% of the recorded data would be null. Therefore, optional sample averaging take advantage of some of the extra 4-Bits, while enhancing the data record precision, lowering noise and reducing data volume [12]. Digitizer characterization indicated less than 1 mV noise voltage (2 counts at 1GS/s), which can be reduced further with sample averaging. With 2V input range, this results in signal-to-noise ratio limit of about 2000. The digitizer's data acquisition software was compiled with LabView and output data is stored in MATLAB compatible binary files, which includes the raw data and housekeeping. Figure 10 shows the GUI of the data acquisition software that run the digitizers to acquire the return signals from both channels as well as the energy monitor channels.

4. IPDA INTEGRATION AND VALIDATION PLANS

The 2-μm IPDA lidar validation is important to assess both CO_2 and H_2O atmospheric measurement capabilities. The IPDA validation is planned to be conducted by comparing the instrument measurements to other gas sensor measurements. Instrument validation will start on ground after instrument integration in the lidar mobile laboratory. The mobile laboratory enables IPDA lidar horizontal measurement using a set calibrated hard targets with different reflectivity, in addition to vertical measurements using clouds as hard target. The main ground validation objectives are to align the instrument and check IPDA operational readiness before aircraft deployment, obtain IPDA signals and noise to evaluate instrument systematic and random errors, compare instrument errors to IPDA models and compare CO_2 and H_2O measurements against correlative *in-situ* instruments, such as CAPABLE, radiosonde, LiCor and Piccaro. Other long term objectives include transferring the laboratory with the instrument to different tall tower sites, such as WLEF tall tower in Park Falls,

Wisconsin, and the Southern Great Plains ARM site in Lamont, Oklahoma. Figure 11 shows the different structures of the whole integrated IPDA lidar instrument. These are the lidar optical structure, including both the laser transmitter and receiver, the electronics rack, mounting the drive and control electronics and the chiller rack for transmitter heat extraction.

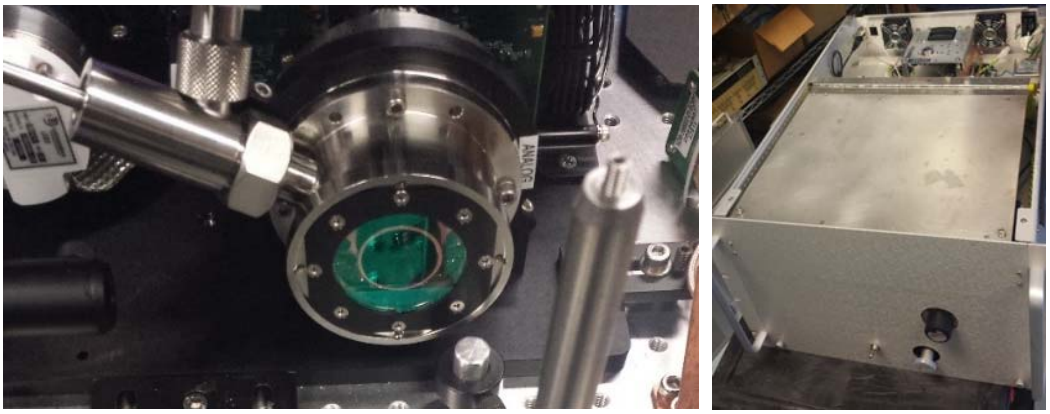

Figure 9. MCT e-APD detector chamber (left) and readout electronics are integrated inside a rack mountable box (right). The box includes a cryo-cooler and vacuum circuit for cooling and thermal isolating the detector.

Figure 20. Graphical user interface of the data acquisition software that runs the digitizers to acquire the return signals from both the InGaAs pin (middle right display) and MCT e-APD detection channels (top right display), as well as the energy monitor channels (top left display).

Figure 12 shows a schematic of the integrated IPDA lidar inside the NASA B-200 aircraft. For airborne operation, the objective of the initial engineering flights would focus on instrument operation and comparing the airborne and ground performance related to signal and noise. Once this is achieved, the objective would focus on comparing CO_2 and H_2O measurements against correlative *in-situ* sensors and models. The validation will rely on onboard sensors (aircraft sensors and LiCor) as well as coordinating and collaborate with science community from other independent sensors, such as

NOAA air-sampling flask flights and Pennsylvania State University passive sensors. At this stage, the main goal is to evaluate and verify both the systematic and the random errors. Airborne validation will be planned to target different conditions such as different surface reflectivity (land, ocean, snow, sand, vegetation) uniform versus variable surface reflectivity, day and night background, clear, cloudy and broken cloud conditions, variable surface elevation and urban pollution and plume detection. The validation may also cover different location such as the Upper Midwest summer, where strong vertical and horizontal spatial gradients in CO_2 occur due to agricultural fluxes and urban deployment in winter, where flight around isolated urban centers could identify a clear atmospheric boundary layer CO_2 plume (for example, near Indianapolis that has an *in-situ* observational network).

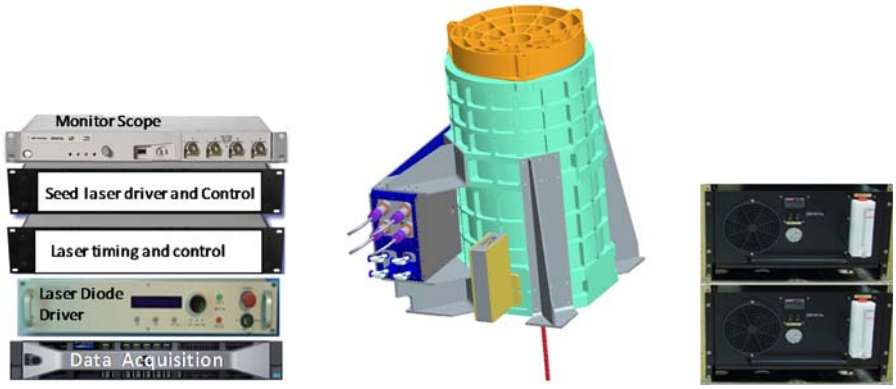

Figure 31. The three structures of the whole integrated IPDA lidar instrument. An electronics rack, mounting the drive and control electronics (left), the lidar optical structure, including both the laser transmitter and receiver (middle), and the chiller rack for transmitter heat extraction (right).

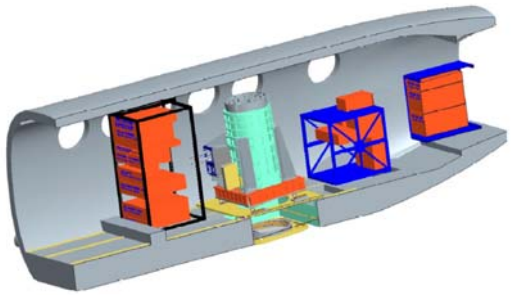

Figure 42. Schematic of the projected IPDA lidar integration inside the NASA B-200 aircraft.

5. CONCLUSIONS FUTURE WORK

A 2-μm double-pulse IPDA lidar instrument have been developed at NASA LaRC. This instrument was validated for active remote sensing of carbon dioxide in the atmosphere. An upgraded, a 2-μm triple-pulse IPDA lidar instrument is being developed at NASA LaRC. This active remote sensor targets and measures both atmospheric carbon dioxide and water vapor. Wavelength selection and laser transmitter operation allows measuring both species independently and simultaneously. This would be the first demonstration of measuring two important greenhouse atmospheric molecules with a single instrument. The basic instrument design is based on knowledge gathered through the previously successful 2-μm double-pulse IPDA. Critical enhancements were implemented in the new triple-pulse design that significantly advance the technology. These enhancements include both the transmitter and receiver. For the transmitter, modifications include high total laser output energy, triple-pulse operation of the laser, laser timing control updates and wavelength control design. In the receiver, updates include telescope integration, data acquisition system and additional high performance e-APD detector. The e-APD detector supplied by NASA GSFC, is a state-of-art, space qualifiable device that

was validated for lidar applications. Combining both the 2-μm triple-pulse transmitter with this new detector in a single instrument will result in a CO_2 IPDA lidar with enabling technology, which meets space requirements. Progress of the 2-μm triple-pulse IPDA program is on schedule. Instrument validation plans are under discussions to collaborate with different research institutes and universities to advance the IPDA lidar technology.

ACKNOWLEDGMENTS

This work was funded by NASA Earth Science Technology Office (Program Director: George Komar and Program Manager: Parminder Ghuman). The authors acknowledge Xiaoli Sun and Luis Ramos-Izquierdo, of NASA Goddard Space Flight Center, in supporting the detection system integration and testing.

REFERENCES

[1] National Research Council, *National Imperatives for the Next Decade and Beyond Committee on Earth Science and Applications from Space: A Community Assessment and Strategy for the Future* (National Academies, 2007).

[2] U. Singh, B. Walsh, J. Yu, M. Petros, M. Kavaya, T. Refaat, and N. Barnes, "Twenty years of Tm:Ho:YLF and LuLiF laser development for global wind and carbon dioxide active remote sensing", Optical Materials Express 5(4), 827 (2015).

[3] G. Koch, J. Beyon, F. Gibert, B. Barnes, S. Ismail, M. Petros, P. Petzar, J. Yu, E. Modlin, K. Davis and U. Singh, "Side-line tunable laser transmitter for differential absorption lidar measurements of CO_2: design and application to atmospheric measurements", Applied Optics 47, 944 (2008).

[4] T. Refaat, S. Ismail, G. Koch, M. Rubio, T. Mack, A. Notari, J. Collins, J. Lewis, R. DeYoung, Y. Choi, N. Abedin and U. Singh, "Backscatter 2-μm Lidar Validation for Atmospheric CO2 Differential Absorption Lidar Applications", IEEE Trans. Geoscience and Remote Sensing 49(1), 572 (2011).

[5] T. Refaat, U. Singh, J. Yu, M. Petros, R. Remus, and S. Ismail, "Double-pulse 2-μm integrated path differential absorption lidar airborne validation for atmospheric carbon dioxide measurement", Applied Optics 55(15), 4232 (2016).

[6] J. Yu, M. Petros, U. Singh, T. Refaat, K. Reithmaier, R. Remus, and W. Johnson, "An airborne 2-μm double-pulsed direct-detection lidar instrument for atmospheric CO_2 column measurements," Journal of Atmospheric and Oceanic Technology 34, 385 (2017).

[7] U. Singh, T. Refaat, J. Yu, M. Petros and R. Remus, "Airborne active remote sensor for atmospheric carbon dioxide", SPIE Newsroom, 2015.

[8] T. Refaat, U. Singh, M. Petros, R. Remus and J. Yu, "Self-calibration and laser energy monitor validation for a double-pulsed 2-μm CO_2 integrated path differential absorption lidar application", Applied Optics 54, 7240 (2015).

[9] T. Refaat, U. Singh, J. Yu, M. Petros, R. Remus and S. Ismail, "Airborne two-micron double-pulse IPDA lidar validation for carbon dioxide measurements over land", 28th International Laser Radar Conference (ILRC), Bucharest, Romania (2017).

[10] T. Refaat, U. Singh, J. Yu, M. Petros, S. Ismail, M. Kavaya, and K. Davis, "Evaluation of an airborne triple-pulsed 2-μm IPDA lidar for simultaneous and independent atmospheric water vapor and carbon dioxide measurements", Applied Optics 54, 1387 (2015).

[11] U. Singh, T. Refaat, M. Petros and J. Yu, "triple-pulsed two-micron integrated path differential absorption lidar: a new active remote sensing capability with path to space," in Proceedings of the 27th International Laser Radar Conference, New York, NY, 2015.

[12] U. Singh, M. Petros, T. Refaat, C. Antill, R. Remus and J. Yu, "Airborne lidar for simultaneous measurement of column CO2 and water vapor in the atmosphere", Proc. SPIE 10006, 1000602 (2016).

[13] U. Singh, T. Refaat, S. Ismail, K. Davis, S. Kawa, R. Menzies and M. Petros, "Feasibility study of a space-based high pulse energy 2 μm CO_2 IPDA lidar", Applied Optics 56(23), 6531 (2017).

[14] B. Walsh, N. Barnes, M. Petros, J. Yu, U. Singh, "Spectroscopy and modeling of solid state lanthanide lasers: Application to trivalent Tm and Ho in YLiF and LuLiF", Journal of Applied Physics 95, 3271 (2004).

[15] M. Petros, T. Refaat, U. Singh, J. Yu, C. Antill, R. Remus, B. Taylor, T. Wong, K. Reithmaier, J. Lee, S. Ismail and K. Davis, "Development of an advanced two-micron triple-pulse IPDA lidar for carbon dioxide and water vapor measurements", 28th International Laser Radar Conference (ILRC), Bucharest, Romania (2017).

[16] T. Refaat, M. Petros, C. Antill, U. Singh and J. Yu, "Wavelength locking to CO_2 absorption line-center for 2-μm pulsed IPDA lidar application", Proc. SPIE 9879, 987904 (2016).
[17] M. Bagheri, G. Spiers, C. Frez, S. Forouhar, and F. Aflatouni, "Linewidth measurement of distributed-feedback semiconductor lasers operating near 2.05 μm," IEEE Photonics Technology Letters 27(18), 1934 (2015).
[18] X. Sun, J. Abshire, J. Beck, 2014: HgCdTe e-APD detector arrays with single photon sensitivity for space lidar applications, Proc. SPIE 9114, 91140K (2014).
[19] X. Sun, J. Abshire, J. Beck, P. Mitra, K. Reiff and G. Yang, "HgCdTe avalanche photodiode detectors for airborne and spaceborne lidar at infrared wavelengths", Optics Express 25(14), 16589 (2017).